



Dynamic Analysis of Planetary Gear Transmission System Considering the Flexibility of Internal Ring Gear

Zhixin Fan¹ · Caichao Zhu¹ · Chaosheng Song¹

Received: 14 May 2018 / Accepted: 14 March 2019 / Published online: 22 March 2019
© Shiraz University 2019

Abstract

A rigid-flexible coupled dynamic model of the planetary gear transmission system was developed considering the flexibility of the internal ring gear (flexible internal ring gear) and the sun shaft based on the shell theory and Timoshenko beam theory, respectively. For the dynamic modeling, the time-varying meshing stiffness and static transmission error excitations were considered and the Runge–Kutta numerical algorithm was applied to calculate the dynamic response. The results indicate that the flexibility of internal ring gear sharply decreases the dynamic factor between the internal ring gear and the planet gear, and it also shows significant positive influences on the system load-sharing performance. For the fixed internal ring gear, the maximum stress is located on the midpoint along the axial direction. The maximum dynamic deformations appear at the ends of the tooth surface along width direction, and the dynamic deformation shows a decremental trend from the tooth top edge to the tooth root edge. The load-sharing coefficient decreases rapidly with the increase in the thickness, as the support stiffness is small. The misalignment of one of the planet pins and various static transmission errors have a negative influence on the load-sharing coefficient of the planetary gear transmission system.

Keywords Planetary gear transmission system · Flexible internal ring gear · Flexible shaft · Dynamic stress and deformation · Load-sharing coefficient

List of symbols

M	Mass
C_d	Damping
K	Stiffness
α	Pressure angle
β	Helical angle
e	Static transmission error
e	Natural constant
X	Displacement
A, B, C	Fourier expanded coefficients
U_v	Elastic strain energy
P_{sp}	Potential energy
T	Kinetic energy
ρ	Density

E	Young's modulus
μ	Poisson's ratio
R_0	Addendum circle radius of the ring gear
R_1	Outer radius of the ring gear
B	Tooth width of the ring gear
x, θ, r	Cylindrical coordinates in the axial, circumferential and radial directions
h	Thickness of the ring gear
\bar{r}	$\bar{r} = r - R_0$
u, v, w	Displacement components
U, V, W	Robust form of the Fourier series expansions
δ	Equivalent displacement
ω	Natural frequency

Subscripts

b	Base circle
c	Carrier
i	Ordinal number
je	Pitch circle
p	Planet gear
r	Ring gear
s	Sun gear
l, g, q	Supplement coefficient

✉ Caichao Zhu
cczhu@cqu.edu.cn
Zhixin Fan
zxfan@cqu.edu.cn
Chaosheng Song
chaoshengsong@cqu.edu.cn

¹ The State Key Laboratory of Mechanical Transmissions, Chongqing University, Chongqing 400044, China

1 Introduction

Planetary gear transmission system is widely used in aerospace, wind power, electric cars and other fields because of the compact structure, light quality, high power density, high carrying capacity, large transmission ratio and high transmission efficiency. The lightweight requirement of the components makes the thin-wall internal ring gear and the hollow sun shaft widely used, and they have obvious effects on the overall performance due to their distinct vibration and deformation. Therefore, to provide a theoretical basis for prolonging its service span, reducing vibration and noise and improving reliability, a thorough dynamic behavior analysis of planetary gear transmission system must be performed, which considers the flexibility of the internal ring gear and sun shaft.

Recently, the dynamics of a planetary gear transmission system has been extensively investigated. Wei et al. (2015) analyzed the dynamic response of a planetary gear transmission system under uncertainty by establishing a torsional planetary dynamic model. Parker and Wu investigated the effect of the internal ring gear and elastic deformations for the ring gear on the parameter stability (Wu 2010; Parker and Wu 2010, 2012). Velex et al. established a dynamic planetary model with a finite element model of the ring gear and analyzed the dynamic response (Abou-sleiman and Velex 2006; Abousleiman et al. 2007). Shao established a planetary bending-torsional coupled dynamic model and investigated the response of the system considering a flexible ring and the plastic deflection of the gear tooth stiffness (Chen et al. 2013). Considering time-varying parameters and a flexible pin, Zhu et al. established a planetary gear dynamic model with the deformation of the flexible pin and analyzed the potential resonance point using the modal energy distribution and order frequency sweep methods (Zhu et al. 2014, 2015). Qiu et al. (2015) developed a coupled dynamic model to investigate the effect of gravity and backlash on the vibration response of the planetary gear transmission system. Helsen et al. (2011, 2014) built a flexible multibody vibration model for a wind turbine gear transmission system considering six degrees of freedom of a bearing and flexible structure. Cooley et al. investigated the vibration and parametric instabilities of rotating elastic rings coupled with the constant and fluctuating fixed discrete stiffness in a high-speed state (Cooley and Parker 2014a, b, 2015; Liu et al. 2017). Zhai et al. (Zhai et al. 2015, 2016) studied the dynamic performance of planetary gear transmission system considering the carrier assembly errors. Wang et al. (Wang et al.

2011) investigated the distinctive wave vibration of a spur ring gear. Shao established a planetary bending-torsional coupling dynamic model and researched impact on the response of the system by considering flexible ring and plastic deflection of gear tooth stiffness (Chen et al. 2013). Yi et al. (Yi et al. 2015) investigated the load-sharing characteristic of planetary gear system considering the meshing error and floating error. Zhang et al. investigated the efforts of assembly errors on the dynamic characteristics of helical planetary gear transmission system (Zhang and Liu 2014). The nonlinear dynamics with mesh phase of the 2D planetary gear system was investigated by Ambarisha and Parker (2007). Guo et al. set up a nonlinear dynamic model for planetary to analyze the effect of gravity on the dynamic response (Guo et al. 2014; Guo and Parker 2010). Ambarisha and Parker (2006) established a numerical model of the planetary gear transmission system to study the nonlinear effects of the mesh phasing on vibration reduction. Erkaya et al. (2007) investigated the kinematic and dynamic analysis of a modified slider–crank mechanism, which has an eccentric connector and drives a planetary gear mechanism. Cooley and Parker (2014b) published a review of literature on planetary gear dynamics. Sun and Hu (2003) established a lateral–torsional coupled model and investigated the nonlinear dynamics of a planetary gear system with multiple clearances. Cervantes-Sánchez and Rico-Martínez (2009) established a planetary gear train model by using multi-bond graph diagrams and verified the validity by resorting to the Lagrange’s equations. Gawande et al. (Gawande and Shaikh 2014; Gawande and Kokare 2017) researched the effect of planet phasing on noise and vibration of a planetary gear system using the experimental work and established an FE planetary gear model to investigate the dynamic analysis. In order to investigate the dynamic behavior of the planetary gear transmission system deeply, many researches discuss the modeling methods and the dynamic behavior considered many factors, like flexibility, errors.

For discussing the effect of the flexibility on the dynamic characteristics of the planetary gear transmission system, in this paper, a rigid-flexible coupled dynamic model of the planetary gear transmission system was developed considering the flexible internal ring gear, flexible shaft, time-varying meshing stiffness and static transmission error excitation. The flexibility of the internal ring gear is based on the shell theory. The dynamic characteristics of the planetary gear transmission system, such as the distribution of dynamic stress and deformation on the pitch line and tooth root of the ring, were investigated.

Fig. 1 Schematic of planetary gear transmission

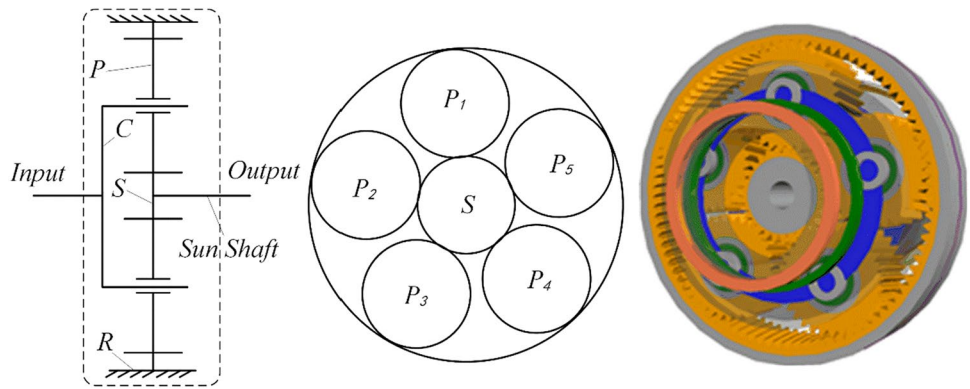


Table 1 Basic parameters of planetary gear transmission system

Item	Ring gear	Sun gear	Planet gear
Number of teeth	91	29	31
Module (mm)	23	23	23
Helix angle (°)	5	5	5
Pressure angle (°)	25	25	25
Tooth width (mm)	505	505	515
Fillet (°)	66	–	–
Mesh stiffness (N/m)	$\bar{K}_{sp}^i = 8.65e9$ $\bar{K}_{rp}^i = 10.9e9$		
Static transmission error (mm)	$e_{sp}^i = 0.022$ $e_{rp}^i = 0.022$		

2 Basic Structure and Parameters of the Planetary Gear Transmission System

A schematic of the planetary gear transmission system as a research object including a rotating carrier *C*, five planet gears P_1, P_2, P_3, P_4, P_5 , a sun gear *S* and a fixed internal ring gear *R* is shown in Fig. 1.

The basic parameters of the planetary gear transmission system, which are from a 5-MW wind turbine gearbox, are listed in Table 1. The time-varying meshing stiffness and the static transmission errors were determined according to the references (Zhai et al. 2016; Sun et al. 2015).

3 Rigid-Flexible Coupled Dynamic Modeling of Planetary Gear Transmission System

3.1 Coupled Modeling for Planetary Gear Transmission System

The modeling methods for the components of planetary gear transmission system are shown in Table 2. The flexible internal ring gear and sun shaft are modeled using the shell theory and finite element method, respectively.



Fig. 2 Schematic of the matrix assembly format

Table 2 Modeling methods for components

Component	Number	Modeling	Usage
Ring (<i>R</i>)	1	Shell theory	Considering structural stiffness and damping
Sun (<i>S</i>)	1	6DOF rigid	–
Sun shaft	1	Finite element method	Connecting sun gear and output and providing torsional stiffness and damping
Planet (<i>P</i>)	5	6DOF rigid	–
Carrier (<i>C</i>)	1	6DOF rigid	–

The equations of a rigid-flexible coupled dynamic model for the planetary gear transmission system are directly expressed according to the rules in Fig. 2. C, R, P and S denote the carrier, ring gear, planet gear and sun gear, respectively. CP, RP and SP are the coupling terms of each component. The dotted rectangular shadow is the flexible sun shaft matrix.

The overall dynamic equation of the planetary gear system can be represented by

$$M\ddot{X} + C\dot{X} + KX = F \tag{1}$$

where M , C and K are the effective mass, damping and stiffness matrices, respectively.

The vibration displacements of the planetary gear transmission system are

$$X = (X_C, X_R, X_{p1}, X_{p2}, X_{p3}, X_{p4}, X_{p5}, X_{Ss}^1, X_S, X_{Ss}^3, X_{Ss}^4, X_{Ss}^5, X_{Ss}^6)^T \tag{2}$$

$$X_R = \begin{pmatrix} A_{00}, \dots, A_{gq}, \dots, A_{GQ}, A_{10}^r, \dots, A_{lg}^r, \dots, A_{2G}^r, A_{10}^x, \dots, A_{lq}^x, \dots, A_{2Q}^x \\ B_{00}, \dots, B_{gq}, \dots, B_{GQ}, B_{10}^r, \dots, B_{lg}^r, \dots, B_{2G}^r, B_{10}^x, \dots, B_{lq}^x, \dots, B_{2Q}^x \\ C_{00}, \dots, C_{gq}, \dots, C_{GQ}, C_{10}^r, \dots, C_{lg}^r, \dots, C_{2G}^r, C_{10}^x, \dots, C_{lq}^x, \dots, C_{2Q}^x \end{pmatrix} e^{i\omega t}$$

$$X_*^{**} = (x_*^{**}, y_*^{**}, z_*^{**}, \theta_{x_*}^{**}, \theta_{y_*}^{**}, \theta_{z_*}^{**})$$

where $A_{gq}, B_{gq}, C_{gq}, A_{lg}^r, B_{lg}^r, C_{lg}^r, A_{lq}^x, B_{lq}^x, C_{lq}^x$ denote the Fourier expanded coefficients and corresponding supplement coefficients for the vibration displacements (Ye et al. 2014). $x_*^{**}, y_*^{**}, z_*^{**}, \theta_{x_*}^{**}, \theta_{y_*}^{**}, \theta_{z_*}^{**}$ represent six degrees of freedoms in the vibration displacements of the rigid components and flexible shaft nodes.

The static coordinates $X_C OY_C$, $X_S OY_S$ and $X_R OY_R$ are defined in the centers of the carrier, sun and ring, respectively. The moving coordinates $X_{pi} OY_{pi}$ are defined in the centers of the planet gears. The locations and relationships of the components are shown in Fig. 3. The supporting stiffness and damping are oriented along the positive direction of the corresponding coordinate. The supporting stiffness and damping matrices are calculated from reference (Zhai et al. 2016).

3.2 Modeling for the Flexible Internal Ring Gear and Sun Shaft

The flexibilities of the internal ring gear and sun shaft are considered for the planetary gear transmission system. The

sun shaft is described by the rotating shaft elements using Timoshenko theory.

As shown in Fig. 4a, the sun shaft is modeled as 5 elements and 6 nodes: Ss1, Ss2, Ss3, Ss4, Ss5 and Ss6. The white nodes Ss2 and Ss5 are connected with the sun gear and load torque. The shaft stiffness and damping matrices are calculated according to references (Chen et al. 2016). For the flexibility, the internal ring gear is modeled as a cylinder shell based on the shell theory (Ye et al. 2014).

The structure schematic and mesh model of the flexible internal ring gear are shown in Fig. 4b. To simplify the model, although the location of the mesh point gradually varies during one mesh cycle, the mesh point between the ring and the planet is assumed to be the midpoint of the pitch line of the internal ring gear. Isotropic material was selected for the modeling of the internal ring gear. The red circles represent the mesh states, which are between each

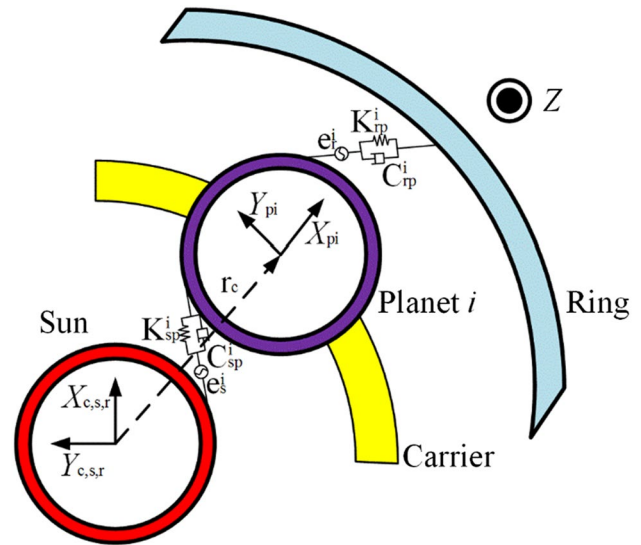
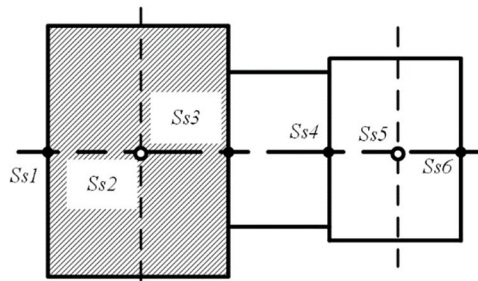


Fig. 3 Dynamic model of the helical planetary transmission

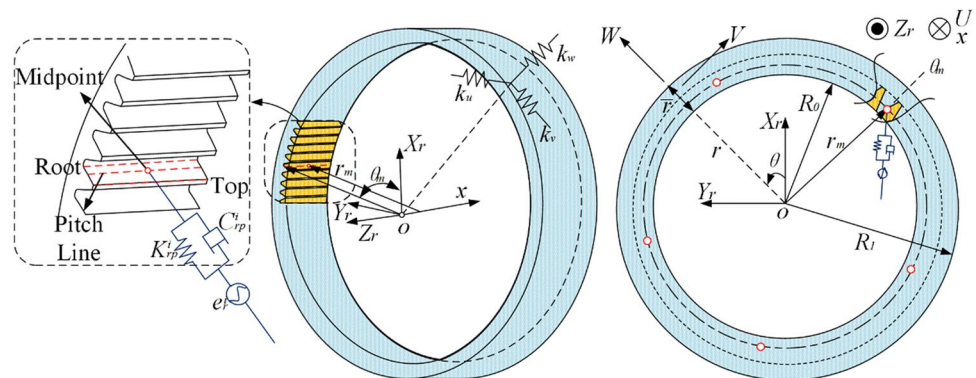
equispaced planet gear and the internal ring gear, and are on the internal ring gear as shown in the figure.

The structural energy expressions of the internal ring gear can be represented by

Fig. 4 Structure schematic of the internal ring gear and the sun shaft



(a) Structure and finite element schematic of the sun shaft



(b) Three-dimensional schematic of the internal ring gear

$$U_v = \frac{E}{4(1 + \mu)} \int_0^B \int_0^h \int_0^{2\pi} \left(\begin{aligned} & \frac{2\mu}{1 - 2\mu} \left(\frac{\partial u}{\partial x} + \frac{\partial v}{(\bar{r} + R_0)\partial\theta} + \frac{w}{\bar{r} + R_0} + \frac{\partial w}{\partial \bar{r}} \right)^2 \\ & + 2 \left(\frac{\partial u}{\partial x} \right)^2 + 2 \left(\frac{\partial v}{(\bar{r} + R_0)\partial\theta} \right)^2 + 2 \left(\frac{\partial w}{\partial \bar{r}} \right)^2 \\ & + \left(\frac{\partial u}{\partial \bar{r}} + \frac{\partial w}{\partial x} \right)^2 + \left(\frac{\partial u}{(\bar{r} + R_0)\partial\theta} + \frac{\partial v}{\partial x} \right)^2 \\ & + \left(\frac{\partial w}{(\bar{r} + R_0)\partial\theta} + \frac{\partial v}{\partial \bar{r}} - \frac{v}{\bar{r} + R_0} \right)^2 \end{aligned} \right) (\bar{r} + R_0) d\theta d\bar{r} dx \quad (3)$$

$$P_{sp} = \frac{1}{2} \int_0^h \int_0^{2\pi} \left\{ \begin{aligned} & (k_{u0}u^2 + k_{v0}v^2 + k_{w0}w^2)|_{x=0} \\ & + (k_{uB}u^2 + k_{vB}v^2 + k_{wB}w^2)|_{x=B} \end{aligned} \right\} d\theta dx \quad (4)$$

$$T = \frac{\rho}{2} \int_0^B \int_0^h \int_0^{2\pi} \left\{ \left(\frac{\partial u}{\partial t} \right)^2 + \left(\frac{\partial v}{\partial t} \right)^2 + \left(\frac{\partial w}{\partial t} \right)^2 \right\} (\bar{r} + R_0) d\theta d\bar{r} dx \quad (5)$$

where U_v , P_{sp} and T are the elastic strain energy, potential energy stored in the boundary springs and kinetic energy of the internal ring gear, respectively. ρ , E and μ are the density, Young's modulus and Poisson's ratio of the material, respectively. h is the thickness from the addendum circle to the outer edge of the ring. R_0 and R_1 are the addendum

circle radius and outer radius of the ring, respectively. B is the tooth width of the ring. X , θ and r are the cylindrical coordinates in the axial, circumferential and radial directions, respectively. u , v and w are the displacement components at any point of the internal ring gear in the axial,

circumferential and radial directions and are expressed in a Fourier series expansion as follows:

$$\begin{cases} u(x, \theta, \bar{r}, t) = U(x, \bar{r}) \cos \theta e^{j\omega t} \\ v(x, \theta, \bar{r}, t) = V(x, \bar{r}) \sin \theta e^{j\omega t} \\ w(x, \theta, \bar{r}, t) = W(x, \bar{r}) \cos \theta e^{j\omega t} \end{cases} \quad (6)$$

where ω is the natural frequency of the ring gear, $j = \sqrt{-1}$. t is time. $\bar{r} \in [0, h]$, $h = R_1 - R_0$. $U(x, \bar{r})$, $V(x, \bar{r})$ and $W(x, \bar{r})$ are the robust form of the Fourier series expansions and are shown as:

$$\begin{cases} U(x, \bar{r}) = \sum_{g=0}^G \sum_{q=0}^Q A_{gq} \cos \lambda_g \cos \lambda_q + \sum_{g=0}^G \sum_{l=1}^2 A_{lg}^r \xi_l(\bar{r}) \cos \lambda_g \\ \quad + \sum_{l=1}^2 \sum_{q=0}^Q A_{lq}^r \xi_l(x) \cos \lambda_g \bar{r} \\ V(x, \bar{r}) = \sum_{g=0}^G \sum_{q=0}^Q B_{gq} \cos \lambda_g \cos \lambda_q + \sum_{g=0}^G \sum_{l=1}^2 B_{lg}^r \xi_l(\bar{r}) \cos \lambda_g \\ \quad + \sum_{l=1}^2 \sum_{q=0}^Q B_{lq}^r \xi_l(x) \cos \lambda_g \bar{r} \\ W(x, \bar{r}) = \sum_{g=0}^G \sum_{q=0}^Q C_{gq} \cos \lambda_g \cos \lambda_q + \sum_{g=0}^G \sum_{l=1}^2 C_{lg}^r \xi_l(\bar{r}) \cos \lambda_g \\ \quad + \sum_{l=1}^2 \sum_{q=0}^Q C_{lq}^r \xi_l(x) \cos \lambda_g \bar{r} \end{cases} \quad (7)$$

Because of the limited computing ability and moderate precision requirement, G and Q are generally 3–5.

The mesh point between the internal ring gear and the i th planet gear is the midpoint of the pitch line on the ring gear. The equivalent displacement between them is

$$\delta_{rp}^i = (x_i - w_i) \sin \alpha_n + (y_i + v_i) \cos \alpha_n \cos \beta + (z_i - u_i) \cos \alpha_n \sin \beta + \theta_i^y r_{pje} \tan \beta_b + \theta_i^z r_{pji} \cos \beta_b + e_{ri} \quad (8)$$

where u_i , v_i and w_i are the displacement components at the mesh point of the internal ring gear in the axial, circumferential and radial directions, respectively. i denotes the planetary gear number, which can be 1–5.

$$\begin{cases} u_i = u(B/2, \theta_m, r_m, t) = U(B/2, r_m) \cos \theta_m e^{j\omega t} \\ v_i = v(B/2, \theta_m, r_m, t) = V(B/2, r_m) \sin \theta_m e^{j\omega t} \\ w_i = w(B/2, \theta_m, r_m, t) = W(B/2, r_m) \cos \theta_m e^{j\omega t} \end{cases} \quad (9)$$

The mesh potential energy between the internal ring gear and the planet gears is

Table 3 Natural frequencies of the planetary gear transmission system

Orders	Present (Hz)	Zhai (Hz)	Masta (Hz)
1	27	31	27
2	63	70	61
3	69	72	69
4	82	88	85
5	95	103	101
6	122	134	123
7	166	185	173
8	202	202	201
9	231	240	226
10	237	244	231

$$U_m = \sum_{i=1}^N \frac{1}{2} K_{rp}^i (\delta_{rp}^i)^2 \quad (10)$$

The Lagrange energy function L can be expressed in terms of the kinetic energy, elastic strain energy, potential energy stored in the boundary springs and mesh potential energy as follows:

$$L = T - U_v - P_{sp} - U_m \quad (11)$$

When the Lagrange energy method is applied, the numbers of equation can be up to $3 * \{(G + 1) * (Q + 1) + 2 * (G + Q + 2)\}$.

4 Dynamic Characteristics Analysis

It is very important to verify the accuracy of the model. The verification method of the reference (Ye et al. 2014) and the reference (Cooley and Parker a, b) is adopted in this paper. The natural frequency of the model is calculated compared with the reference (Zhai et al. 2016) and the finite element method as shown in Table 3.

By comparing with the methods and results published by Zhai et al., a close agreement between these two results can be found. Although different modeling method was used in the reference, the professional software Masta used in this paper is based on the finite element method (FEM). Comparing with the results gotten from the FEM, the present results are closer to the results from the Masta.

Based on the coupled dynamic model shown above, the Runge–Kutta numerical algorithm was applied to calculate the dynamic responses. Under the rated load conditions of a 5-MW wind turbine gearbox (the input torque is 48,800 Nm, and the input rotation speed is 11.34 rpm), the dynamic

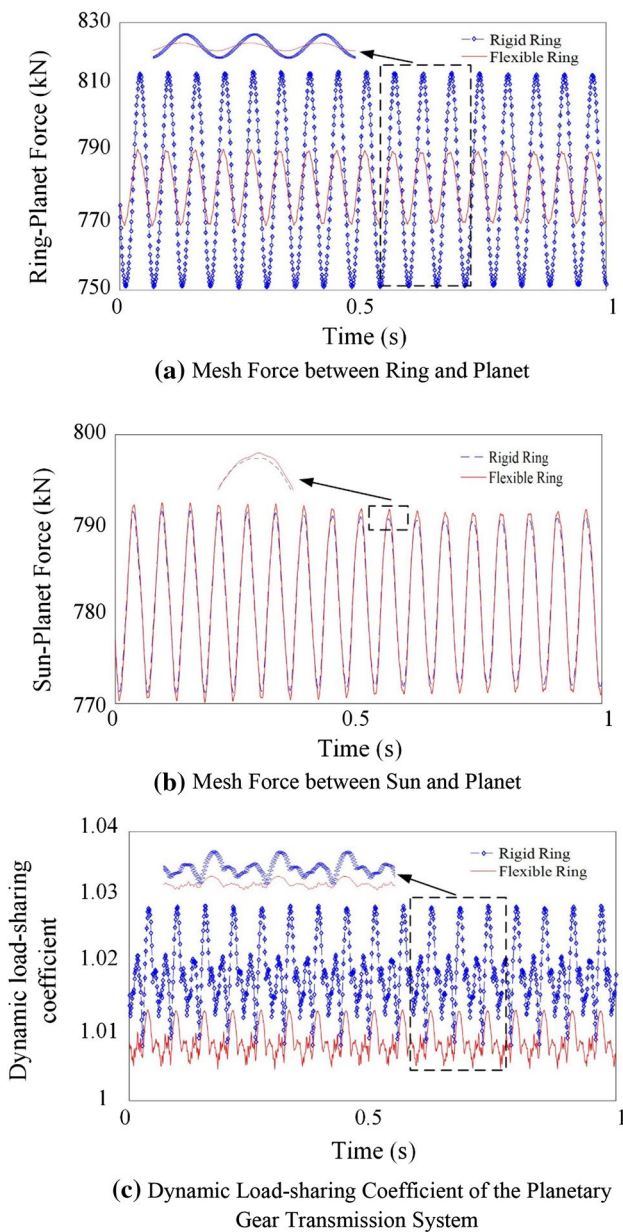
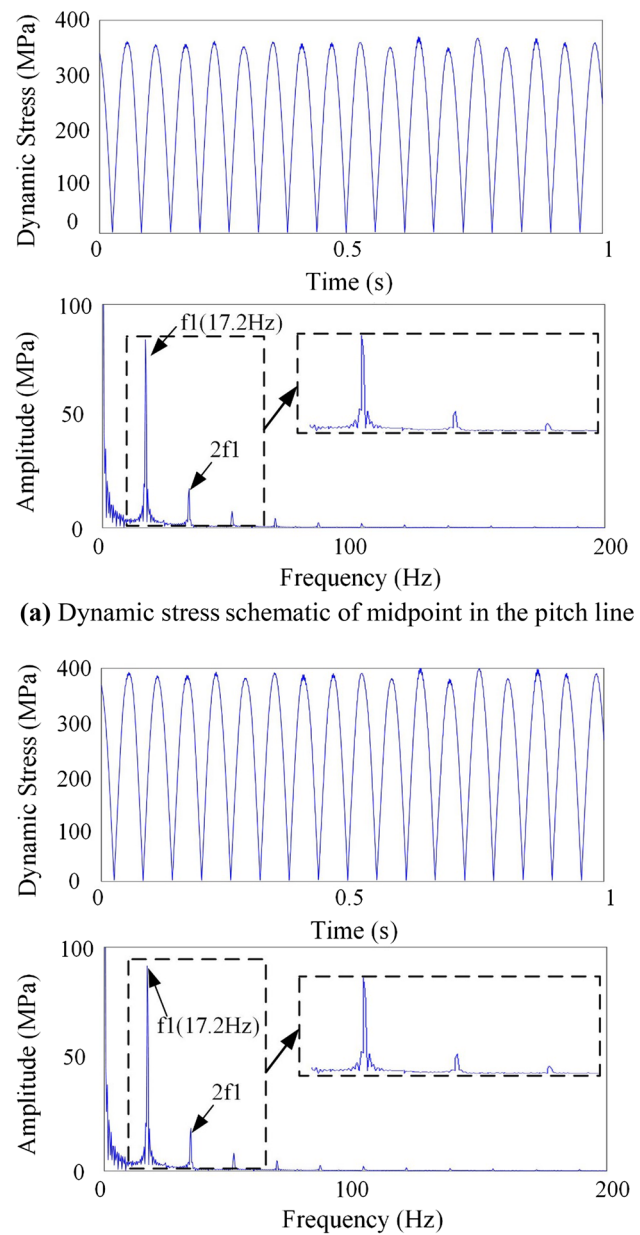


Fig. 5 Comparison schematic of the dynamic meshing forces and load-sharing coefficient

mesh forces and load-sharing performance of planetary gear transmission system are compared for the dynamic model with (flexible) and without (rigid) considering the flexibility of the internal ring gear. The dynamic mesh forces F_{rp} (Ring-Planet gear) and F_{sp} (Sun-Planet gear) are shown in Fig. 5a, b. The dynamic load-sharing coefficient of the planetary gear transmission is shown in Fig. 5c.

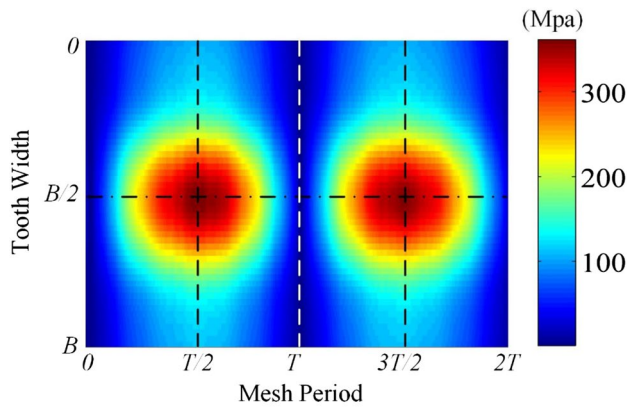
The flexibility of the internal ring gear sharply affects the maximum value and the vibration amplitude of F_{rp} . The flexibility of the internal ring gear scarcely affects the maximum value and vibration amplitude of F_{sp} . It can be



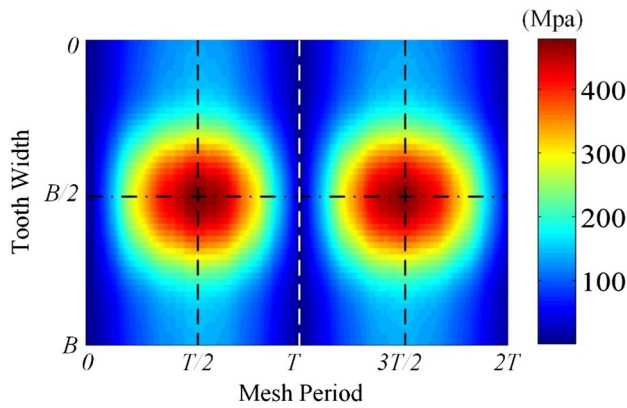
(a) Dynamic stress schematic of midpoint in the pitch line

(b) Dynamic stress schematic of midpoint in the tooth root

seen that the flexibility of the internal ring gear shows obvious influence on the peak–peak value of the F_{rp} . But the flexibility of internal ring gear scarcely ever effects on the peak–peak value of the F_{sp} . The maximum value of the F_{rp} has been decreased by 3.2%, and the maximum value of F_{sp} has been increased a little. The dynamic factor between the internal ring gear and the planet gear decreases from 1.045 to 1.020, and the dynamic factor between the sun gear and the planet gear slightly increases. The maximum load-sharing coefficient decreases from 1.029 to 1.0129 when the



(a) The Pitch Line



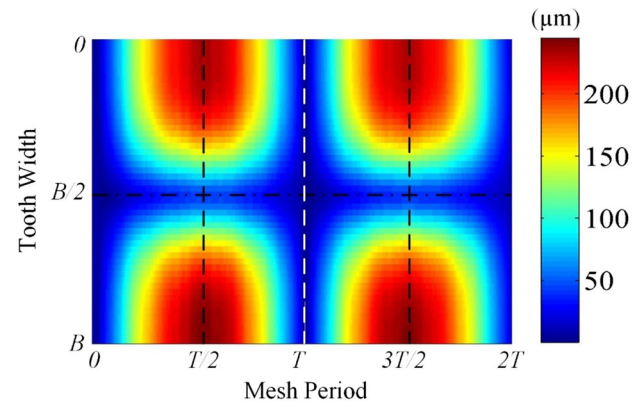
(b) The Tooth Root

Fig. 7 Dynamic stress distribution in the pitch line and the tooth root of the fixed internal ring gear

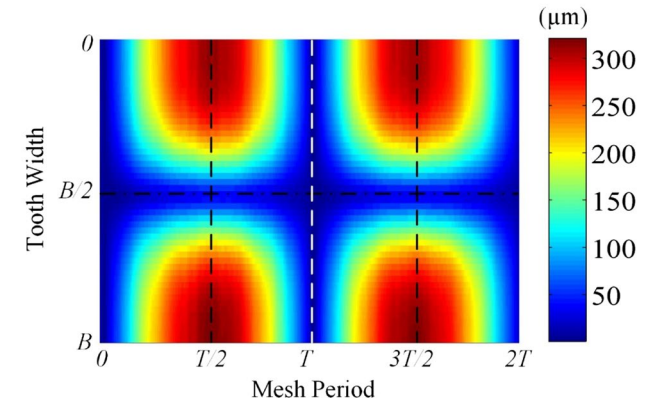
flexible internal ring gear is considered. The flexibility of the internal ring gear makes a significant effect on the dynamic factor between the internal ring gear and the planet gear as well as the load-sharing coefficient.

The dynamic von Mises stress and deformation for the pitch line, tooth top and tooth root of the internal ring gear in planetary gear transmission were analyzed. The dynamic stress in the time and frequency domains of the midpoints for the pitch line and the tooth root (Fig. 4b) can be solved using Eqs. (6) and (9). The results include the dynamic stress of midpoint in the pitch line and the tooth root, respectively, as shown in Fig. 6.

The maximum stress values of the midpoint for the pitch line and the midpoint for the tooth root are 366 MPa and 485 MPa, respectively. The spectra show that the main frequency components are f_1 and $2f_1$ ($f_1 = 17.2$ Hz is the mesh frequency). A meshing course of the helical gear tooth is from the top to the end (the root to the top), from one end of the tooth to the other end. To simplify the model and the factors, the meshing process of a helical gear is equivalent to the time-varying mesh stiffness and the equivalent



(a) The Pitch Line



(b) The Tooth Top

Fig. 8 Dynamic deformation distribution for the pitch line and the tooth top of the fixed internal ring gear

displacement between the internal ring gear and the planet gear. And the mesh state is assumed to be the midpoint of the pitch line of the internal ring gear. Like a beam, the stress of the tooth root is larger than the stress of the pitch line. The dynamic stress distributions for the pitch line and the tooth root of the fixed internal ring gear are shown in Fig. 7. The horizontal axis represents mesh period T . The vertical axis represents the pitch line and the tooth root of the internal ring gear along the tooth width. 0 and B denote the front end and back end of the internal ring gear, respectively. The dash and dot lines at $B/2$ imply the stress variation of the midpoint for the pitch line.

From the results, the minimum dynamic stress for the pitch line and the tooth root of the fixed internal ring gear can be obtained for the time 0 and T , and the maximum dynamic stress is located at the time $T/2$ and the time $3T/2$. The dynamic stress varies periodically. The maximum dynamic stress value of the pitch line is on the midpoint because the contact region between the internal ring gear and the planet gear is assumed to be the midpoint of pitch line. Like a beam, the stress of the tooth root is larger than the stress of the pitch line. The dynamic stress of the pitch

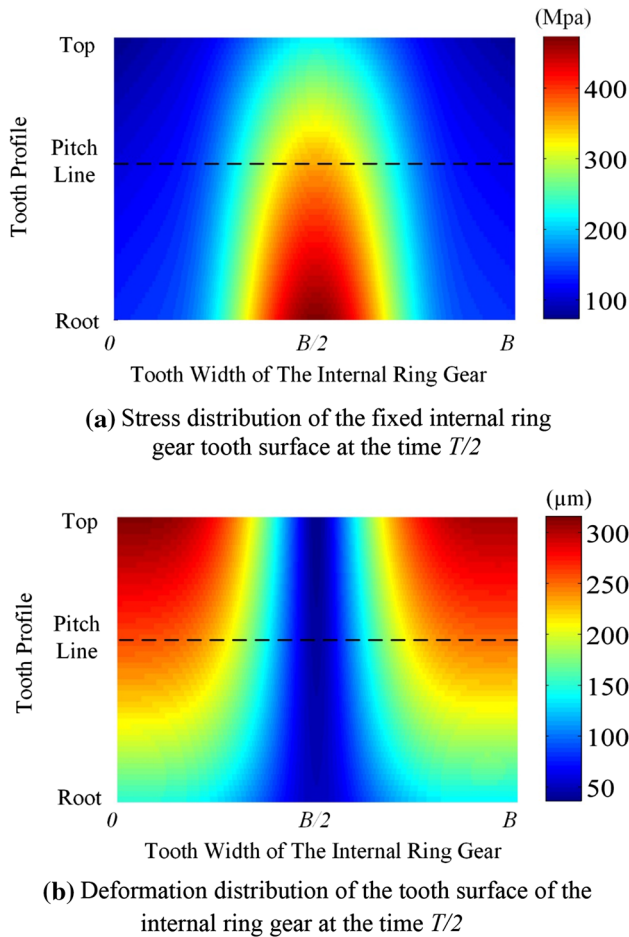


Fig. 9 Stress and deformation distribution of the tooth surface of the internal ring gear

Table 4 Different support stiffness of the internal ring gear

Item	Transverse stiffness (N/m)	Axial stiffness (N/m)
Low support stiffness	6e10	2e10
Mediate support stiffness	18e10	6e10
High support stiffness	30e10	10e10

line and the tooth root is symmetric about the midpoint and gradually declines to both ends of the tooth width. The dynamic deformation distributions for the pitch line and the tooth top of the fixed internal ring gear are shown in Fig. 8.

The minimum dynamic deformation for pitch line and tooth top of the internal ring gear is located at the time 0 and T . The maximum dynamic deformation is at the time $T/2$ and the time $3T/2$. The dynamic deformation varies periodically. The maximum deformation for both the pitch line and the tooth top appear at the ends of the internal

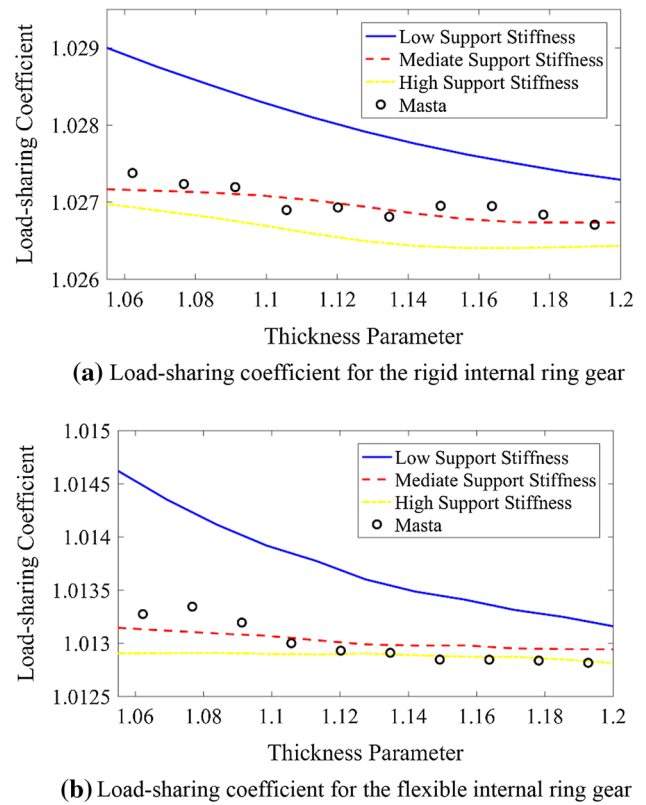
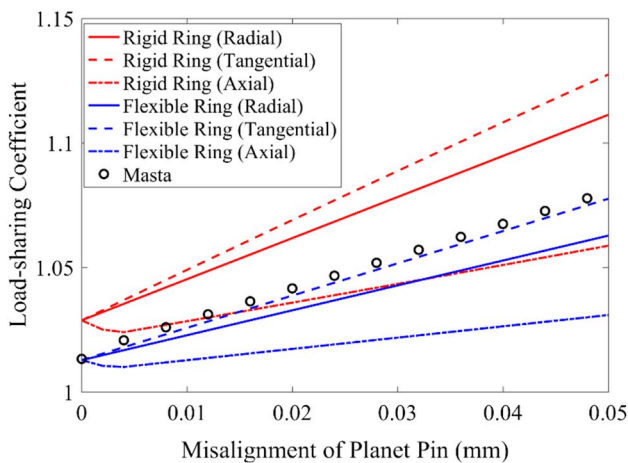


Fig. 10 Load-sharing coefficient of the planetary gear transmission system with various thickness parameters in different boundary spring conditions

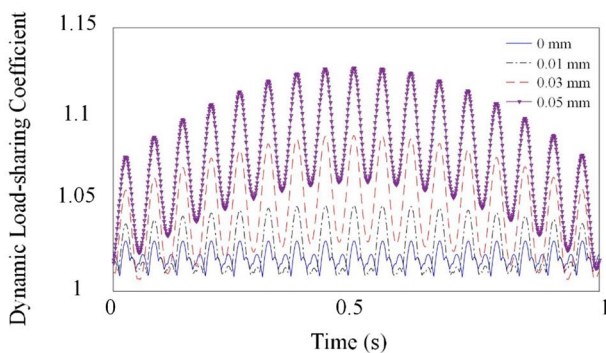
ring gear tooth along the width direction. The deformation of the tooth top is larger than the deformation of the pitch line. The dynamic deformation of the pitch line and the tooth top is symmetric about the midpoint and gradually increases to both ends along the tooth width direction. The stress and deformation distribution of the tooth surface at the time $T/2$ is shown in Fig. 9.

The results show that the stress gradually increases from tooth top edge to tooth root edge. The stress distribution is symmetric around the centerline of the tooth surface and the maximum value on the midpoint of the tooth root (at $B/2$) is 485 MPa, which is 25% larger than the value for the midpoint of the pitch line. The stress mainly appears in the middle of the tooth width. The deformation gradually increases from tooth root edge to tooth top edge. The deformation distribution is symmetric around the centerline of the tooth surface, and the maximum deformation at both ends of the tooth top is 316 μm . The deformation exceeds 250 μm in approximately 25% of the tooth surface. The deformation mainly appears in both ends of the tooth width.

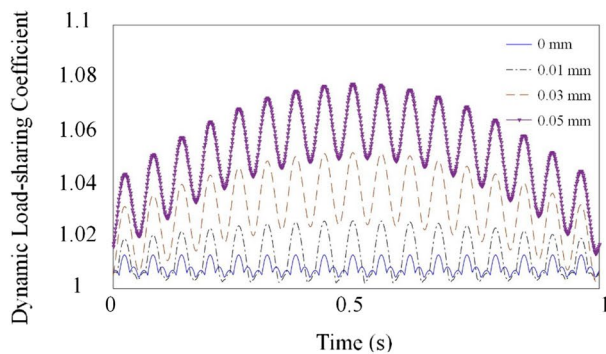
For simplicity and convenience in the analysis, the thickness parameter γ , which is defined as the outer–inner ratio of the internal ring gear, is introduced here ($\gamma = R1/R0$). The



(a) Load-sharing coefficients with different misalignments of one planet pin



(b) Dynamic load-sharing coefficient for the rigid internal ring gear



(c) Dynamic load-sharing coefficient for the flexible internal ring gear

Fig. 11 Comparison schematic of the load-sharing coefficient

different support stiffness of the internal ring gear is listed in Table 4.

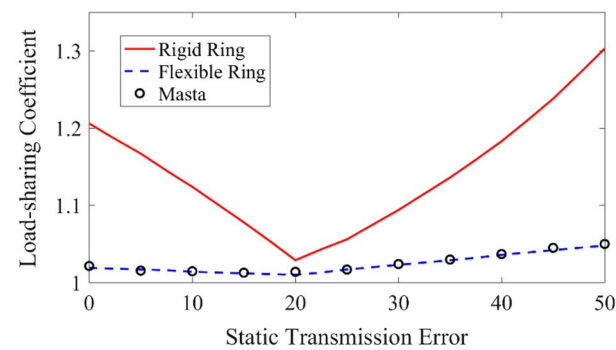
The effects of support stiffness of the different boundary spring conditions on the internal ring gear with the different thickness parameters are investigated as shown in Fig. 10.

The load-sharing coefficients (the maximum) of the planetary gear transmission system almost remain constant

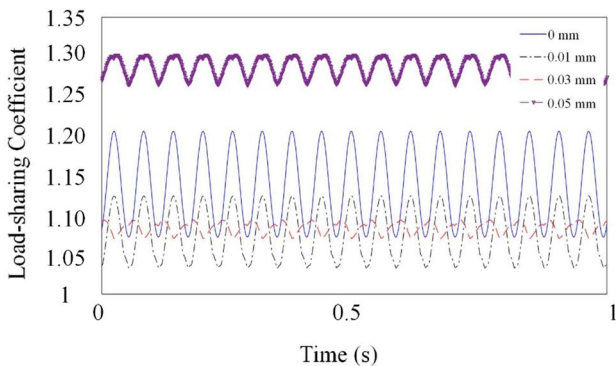
when the support stiffness is moderate and high, the change of the thickness parameter has little effect on the load-sharing coefficient of the planetary transmission system. However, as the support stiffness decreases, a distinct influence can be observed, in which the load-sharing coefficient decreases rapidly with the increase in the thickness parameter. The influences of misalignments of one of the planet pins on the load-sharing coefficients are shown in Fig. 11a. The dynamic load-sharing coefficients of the planetary gear transmission system with the different misalignments of the planet pin in time domain for the internal ring gear are shown in Fig. 11b, c.

The definition of the misalignment of the planet pin is from reference (Zhai et al. 2016). The misalignments from 0 to 0.05 mm along the radial direction, tangential direction and axial direction of one planet pin have a negative effect on the load-sharing coefficient of the planetary gear transmission system. And the misalignment of the planet pin along the tangential direction has the most significant influence on the load-sharing coefficient for the internal ring gear. With the increase in the radial misalignment quantities from 0 mm to 0.05 mm, the load-sharing coefficient of the planetary gear transmission system with rigid ring gear is increased from 1.03 to 1.10 and the load-sharing coefficient of the planetary gear transmission system with flexible ring gear is increased from 1.015 to 1.05. With the increase in the tangential misalignment quantities from 0 to 0.05 mm, the load-sharing coefficient of the planetary gear transmission system with rigid ring gear is increased from 1.03 to 1.12 and the load-sharing coefficient of the planetary gear transmission system with flexible ring gear is increased from 1.015 to 1.065. With the increase in the axial misalignment quantities from 0 to 0.05 mm, the load-sharing coefficient of the planetary gear transmission system with rigid ring gear is increased from 1.03 to 1.046 and the load-sharing coefficient of the planetary gear transmission system with flexible ring gear is increased from 1.015 to 1.02. With the increase in the tangential misalignment quantities from 0 to 0.05 mm, the dynamic load-sharing coefficient of the planetary gear transmission system becomes larger and the amplitude increases obviously. After considering the flexibility of the internal ring gear, the load-sharing performance becomes better. The influences of various static transmission errors between one planet gear and the internal ring gear on the load-sharing coefficient of the planet gear transmission system are shown in Fig. 12.

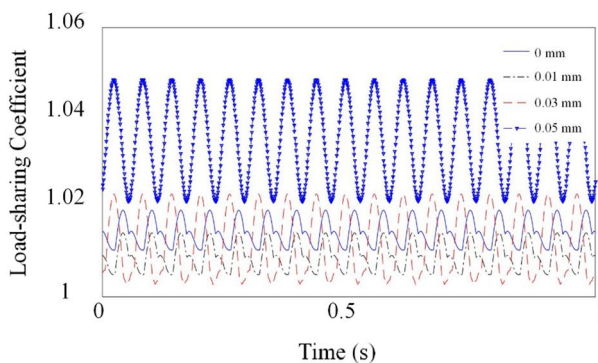
With the increase in the static transmission error quantities from 0 to 0.022 mm, the load-sharing coefficient of the planetary gear transmission system with rigid ring gear is decreased from 1.20 to 1.03. With the increase in the static transmission error quantities from 0.022 to



(a) Load-sharing coefficient with various static transmission errors



(b) Dynamic load-sharing coefficient for the rigid internal ring gear



(c) Dynamic load-sharing coefficient for the flexible internal ring gear

Fig. 12 Load-sharing coefficient with various static transmission errors for the rigid and flexible internal ring gear

0.05 mm, the load-sharing coefficient of the planetary gear transmission system with rigid ring gear is increased from 1.03 to 1.27. The load-sharing coefficients of the planetary gear transmission system for the rigid internal ring gear decrease fast when the static transmission error between one planet gear and the internal ring gear approaches 0.022 mm, which is equal to the static

transmission errors between other planet gears and the internal ring gear. As it further increase, the load-sharing coefficients increase rapidly. After considering the flexibility of the internal ring gear, the static transmission error has less effect on the dynamic load-sharing coefficient of the planetary gear transmission system.

5 Conclusions

In this paper, considering the flexibility of the internal ring gear and shaft, the time-varying meshing stiffness and the system transmission error excitations, a rigid-flexible coupled dynamic model of planetary gear transmission system has been developed, and the Runge–Kutta numerical algorithm was used to calculate the dynamic response. The main conclusions are summarized as follows:

1. When the flexibility of the internal ring gear is considered in the dynamic model, the system load-sharing performance is improved obviously. The dynamic factor between the internal ring gear and the planet gear decreases from 1.045 to 1.020, and the dynamic factor between the sun gear and the planet gear slightly increases.
2. The maximum stress of the internal ring gear tooth is located at the midpoint along the width of the ring tooth root. The maximum stress of the tooth root in the internal ring gear is higher than the maximum stress of the pitch line. The stress of the internal ring gear tooth surface gradually increases from tooth top edge to tooth root edge. The maximum deformation of the pitch line and tooth top in the internal ring gear is located at the ends of the tooth surface along the tooth width direction, and the dynamic deformation shows an incremental trend from the tooth root edge to the tooth top edge.
3. When the support stiffness is mediate and high, the change of the thickness of the internal ring gear has little effect on the load-sharing coefficient of the planetary transmission system. As the support stiffness decreases, the load-sharing coefficient decreases rapidly with the increase in the thickness. The misalignment of one planet pin and various static transmission errors have a negative effect on the load-sharing coefficient, and the tangential misalignment has greatest influence on the load-sharing coefficient.

Acknowledgements The authors appreciate the financial support from the National Natural Science Foundation of China (Grant Nos. 51405043, 51575060) and Chongqing Innovation Program (Nos. cstc2015zdcy-ztxx70010, cstc2015zdcy-ztxx70012).

References

- Abousleiman V, Velex P (2006) A hybrid 3D finite element/lumped parameter model for quasi-static and dynamic analyses of planetary/epicyclic gear sets. *Mech Mach Theory* 41(6):725–748
- Abousleiman V, Velex P, Becquerelle S (2007) Modeling of spur and helical gear planetary drives with flexible ring gears and planet carriers. *J Mech Des* 129(1):95–106
- Ambarisha VK, Parker RG (2006) Suppression of planet mode response in planetary gear dynamics through mesh phasing. *J Vib Acoust* 128(2):133–142
- Ambarisha VK, Parker RG (2007) Nonlinear dynamics of planetary gears using analytical and finite element models. *J Sound Vib* 302(3):577–595
- Cervantes-Sánchez JJ, Rico-Martínez JM (2009) Simulation of planetary gear trains, modeling and numerical validation. *Proc Inst Mech Eng K J Multibody Dyn* 223:53–71
- Chen ZG, Shao YM, Su DZ (2013) Dynamic simulation of planetary gear set with flexible spur ring gear. *J Sound Vib* 332(26):7191–7204
- Chen SY, Tang JY, Li YP et al (2016) Rotordynamics analysis of a double-helical gear transmission system. *Meccanica* 51(1):251–268
- Cooley CG, Parker RG (2014a) Vibration of high-speed rotating rings coupled to space-fixed stiffnesses. *J Sound Vib* 333(12):2631–2648
- Cooley CG, Parker RG (2014b) A review of planetary and epicyclic gear dynamics and vibrations research. *Appl Mech Rev* 66(4):040804
- Cooley CG, Parker RG (2015) Limitations of an inextensible model for the vibration of high-speed rotating elastic rings with attached space-fixed discrete stiffnesses. *Eur J Mech A Solids* 54:187–197
- Erkaya S, Su Ş, Uzmay İ (2007) Dynamic analysis of a slider–crank mechanism with eccentric connector and planetary gears. *Mech Mach Theory* 42(4):393–408
- Gawande S, Kokare DK (2017) Experimental investigations of vibration reduction in spur gear pair by method of phasing. *J Vib Eng Technol* 5(6):13
- Gawande SH, Shaikh SN (2014) Experimental investigations of noise control in planetary gear set by phasing. *J Eng* 2014:1–11
- Guo Y, Parker RG (2010) Sensitivity of general compound planetary gear natural frequencies and vibration modes to model parameters. *J Vib Acoust* 132(1):647–670
- Guo Y, Keller J, Parker RG (2014) Nonlinear dynamics and stability of wind turbine planetary gear sets under gravity effects. *Eur J Mech A Solids* 47:45–57
- Helsen J, Vanhollebeke F, De Coninck F et al (2011) Insights in wind turbine drive train dynamics gathered by validating advanced models on a newly developed 13.2 MW dynamically controlled test-rig. *Mechatronics* 21(4):737–752
- Helsen J, Peeters P, Vanslambrouck K et al (2014) The dynamic behavior induced by different wind turbine gearbox suspension methods assessed by means of the flexible multibody technique. *Renewable Energy* 69:336–346
- Liu CG, Cooley CG, Parker RG (2017) Parametric instability of spinning elastic rings excited by fluctuating space-fixed stiffnesses. *J Sound Vib* 400:533–549
- Parker RG, Wu X (2010) Vibration modes of planetary gears with unequally spaced planets and an elastic ring gear. *J Sound Vib* 329(11):2265–2275
- Parker RG, Wu XH (2012) Parametric instability of planetary gears having elastic continuum ring gears. *J Vib Acoust* 134(4):1–11
- Qiu XH, Han QK, Chu FL (2015) Load-sharing characteristics of planetary gear transmission in horizontal axis wind turbines. *Mech Mach Theory* 92:391–406
- Sun T, Hu HY (2003) Nonlinear dynamics of a planetary gear system with multiple clearances. *Mech Mach Theory* 38(12):1371–1390
- Sun W, Li X, Wei J et al (2015) A study on load-sharing structure of multi-stage planetary transmission system. *J Mech Sci Technol* 29(4):1501–1511
- Wang SY, Huo MN, Zhang C et al (2011) Effect of mesh phase on wave vibration of spur planetary ring gear. *Eur J Mech A Solids* 30(6):820–827
- Wei S, Zhao JS, Han QK et al (2015) Dynamic response analysis on torsional vibrations of wind turbine geared transmission system with uncertainty. *Renewable Energy* 78:60–67
- Wu XH (2010) Vibration of planetary gears having an elastic continuum ring gear dissertation. Ph.D. thesis, Ohio State University, USA
- Ye TG, Jin GY, Shi SX et al (2014) Three-dimensional free vibration analysis of thick cylindrical shells with general end conditions and resting on elastic foundations. *Int J Mech Sci* 84:120–137
- Yi PX, Zhang C, Guo LJ et al (2015) Dynamic modeling and analysis of load sharing characteristics of wind turbine gearbox. *Adv Mech Eng* 7(3):1–16
- Zhai HF, Zhu CC, Song CS et al (2015) Dynamic modeling and analysis for transmission system of high-power wind turbine gearbox. *J Mech Sci Technol* 29(10):4073–4082
- Zhai HF, Zhu CC, Song CS et al (2016) Influences of carrier assembly errors on the dynamic characteristics for wind turbine gearbox. *Mech Mach Theory* 103:138–147
- Zhang J, Liu XZ (2014) Multibody dynamic modeling and analysis for a helical planetary gear train. *J Vib Shock* 33(7):11–17
- Zhu CC, Xu XY, Liu HJ et al (2014) Research on dynamical characteristics of wind turbine gearboxes with flexible pins. *Renewable Energy* 68(7):724–732
- Zhu CC, Chen S, Song CS et al (2015) Dynamic analysis of a megawatt wind turbine drive train. *J Mech Sci Technol* 29(5):1913–1919